Accurate Characterization of Rotor Activity during Atrial Fibrillation Depends on the Properties of the Multi-electrode Grid

Laura Martínez [1], Lucía Romero [1], Catalina Tobón [2], José M Ferrero [1], José Jalife [3], Omer Berenfeld [3], Javier Saiz [1]

[1]I3BH, Universidad Politécnica de Valencia, Valencia, Spain
[2]GI2B, Instituto Tecnológico Metropolitano, Medellín, Colombia
[3]Center for Arrhythmia Research, University of Michigan, Ann Arbor, Michigan, USA

Abstract

Multi-electrode array systems are increasingly being used to study atrial electrical excitation in humans and are shedding new light on the mechanisms of atrial fibrillation (AF). However the mapping systems that are currently being used to characterize the rotors that are postulated to drive AF have not been systematically analyzed for accuracy.

Computer simulations of chronic AF (cAF) were carried out using a realistic 3D model of the atria. Extracellular electrical potentials were calculated on intra-atrial electrode arrays placed at the driving rotor area. The array-to-endocardial wall distance (d_{aew}) was set at 0.2, 1, 2 and 5 mm and uniform interelectrode-distances (d_{ie}) were set at 1, 2 or 5 mm. The instantaneous location of the rotor meandering were analyzed on interpolated phase movies based on the Hilbert transform.

At d_{ie} of 1 mm and $d_{aew} \leq 2$ mm, the rotor location on the array was not significantly different from that on the wall, although meandering on the array was greater than in the atrium. At $d_{ie} = 2$ mm, increasing the d_{aew} decreased the detected meandering area, but remained higher than in the atrium. Finally, when the spatial resolution was 5 mm, in most cases the array recognized the presence of the rotor, but not its trajectory accurately.

1. Introduction

Atrial fibrillation (AF) is the leading cardiac arrhythmia seen in clinical practice. About 2.3 million people in the USA and 4.5 million people in European Union have AF [1-2]. Still, the mechanisms maintaining AF are not well understood. Therefore, it is of great importance to develop new technologies aimed at better identifying and targeting AF sources and help physicians improve treatment procedures, and thereby achieve a better quality of life for patients.

Multi-electrode array systems are increasingly being used to study atrial electrical excitation in humans, with the idea of obtaining spatio-temporal maps used as diagnostic tools to improve efficacy of ablation procedures [3-4]. However, the mapping systems that are currently being used to characterize the rotors that are postulated to be the organizing centers of reentry and drivers of AF have not been systematically analyzed for accuracy.

Here we use computer simulations to quantify the effect of an intra-atrial multi-electrode grid configuration on the accuracy of detecting rotors and their meandering.

2. Methods

2.1. Computer simulations

A previously developed realistic 3D model of the human atria [5-6], including fiber orientation, anisotropy and electrophysiological heterogeneity, was used to carry out computer simulations of chronic AF (cAF). This model consists of the following anatomical structures: left atrium (LA), right atrium (RA), pectinate muscles (PM), crista terminalis (CT), left and right atrial appendages (LAA, RAA), left and right pulmonary veins (LPV, RPV), superior and inferior caval veins (SCV, ICV), coronary sinus (CS), Bachmann's bundle (BB), fossa ovalis (FO), isthmus, tricuspid valve ring (TVR) and mitral valve ring (MVR). The geometric mesh comprises 52,906 hexahedral elements and 100,554 nodes.

A modified version of the Courtemanche et al model [7] was used to reproduce the cellular electrical activity under cAF conditions, based on experimental data of Van Wagoner [8] (see Table 1).

Simulations were carried out generating cAF by two S1-S2 protocols. S1 simulated impulses of sinus origin consisting of a train of stimuli applied to the sinus node region at a basic cycle length of 500 ms for 2500 ms. In the first simulation (cAF1), S2 was a train of 5 ectopic stimuli applied at the superior RPV at a cycle length of 90

ms. In the second simulation (cAF2) S2 consisted of a continuous train of stimuli with a cycle length of 90 ms. Both protocols yielded stable rotors in the free wall of the LA.

Table 1. Conductance (g) changes of currents for cAF

Conductance	cAF (Relative to [7])
g_{K1}	Increased by 100%
g_{Kur}	Decreased by 50%
g_{to}	Decreased by 50%
g_{CaL}	Decreased by 70%

The electrical propagation of action potentials (AP) in the tissue was obtained by solving the mono-domain reaction-diffusion equation

$$\frac{1}{S_v} \nabla \cdot (D \nabla V_m) = C_m \frac{\partial V_m}{\partial t} + I_{ion} - I_{stim} \qquad (1)$$

with the finite elements method [9]. In Eq. (1), Sv is the surface-to-volume ratio, D the conductivity tensor, V_m the membrane potential, C_m the membrane capacitance, I_{ion} the sum of all the ionic currents flowing through the membrane and I_{stim} the stimulus current.

Unipolar electrograms (EGM) were calculated, with a temporal resolution of 1 ms, by computing the extracellular potential in an approximate large volume conductor as:

$$\phi_e(r) = -\frac{\gamma}{4\pi} \cdot \frac{\sigma_i}{\sigma_e} \iiint \nabla' V_m(r') \cdot \nabla' \left[\frac{1}{r'-r}\right] dv \qquad (2)$$

where $\gamma < 1$ is a scale factor (the total volume of the myocardium is greater than the intracellular volume of the fibers), σ_i and σ_e are the intracellular and extracellular conductivities, $\nabla' Vm$ is the gradient of the transmembrane potential (Vm), r' is the distance from the origin to the source point (x', y', z'), r is the distance from the origin to the measuring point (x, y, z) and dv is the differential volume [10].

2.2. Multi-electrode arrays

Virtual intra-atrial multi-electrode arrays, placed at the driving rotor area (see black square on the LA in Figure 1), were constructed to simulate mapping those rotors using multiple extracellular electrical potential (2) recordings. The array-to-endocardial wall distance (d_{aew}) was set at 0.2, 1, 2 and 5 mm and the interelectrode-distance (d_{ie}) was set at 1, 2 or 5 mm (spatial resolution).

At a d_{ie} of 1 mm, the array included 22×22 electrodes, whereas at 2 and 5 mm, the array contained 11×11 and 5×5 electrodes respectively, as shown in Figure 1.
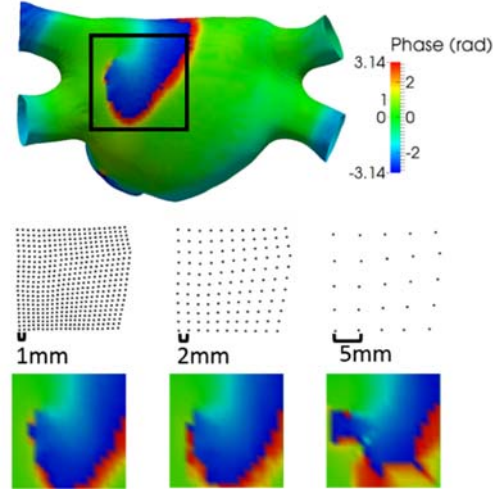

Figure 1. Top and middle, phase map on the LA and multi-electrode arrays (d_{ie}: 1, 2 and 5 mm). The black square over the LA indicates the driving rotor area where arrays were placed. Bottom, phase maps obtained by placing the respective arrays at a distance of 0.2 mm from the endocardial surface (cAF1 simulation).

An EGM was obtained for each electrode of the array. Then, EGMs were interpolated in order to have the same number of EGMs in all cases (linear interpolation), and phase maps based on the Hilbert transform were obtained [4, 11-13]. Finally, phase singularities (PS) were detected at sites exhibiting:

$$\oint \nabla\theta \cdot dr = \pm 2\pi \qquad (3)$$

$\nabla\theta$ is the gradient of the instantaneous phase along a closed path surrounding the possible pivoting point. Points satisfying Eq. (3) were used to analyze the rotor meandering area (A) [14-15].

3. Results

Increasing the distance between the array and the endocardium decreased the EGM amplitude (30-58% for d_{aew}=1 mm, 58-73% for d_{aew}=2 mm and 75-87% for d_{aew}=5 mm).

Figure 2 shows the meandering area A calculated on the atria (A_{cAF1}=0.3 cm^2 and A_{cAF2}=0.45 cm^2) and on each multi-electrode array configuration as a function of the array-to-endocardial wall distance. Black dashed lines indicate 50 and 100% increase in the meandering area.

At a spatial resolution of 1 mm and $d_{aew} \leq 2$ mm, the rotor location on the array was not significantly different from that in the endocardial surface itself, as shown in Table 2, although the meandering area on the array was larger than in the atrium ($A_{cAF1} \approx 0.4$ and $A_{cAF2} \approx 0.5$ cm^2).

However, for d_{aew}>2 mm the meandering area was larger in cAF1 (0.92 cm^2) and smaller in cAF2 (0.28 cm^2). In the latter case, the smaller area was due to the lower number of PS detections (3727 vs 3801 in the atria). This means that from the 3801 ms analyzed, only in 3727 instants a PS was detected.
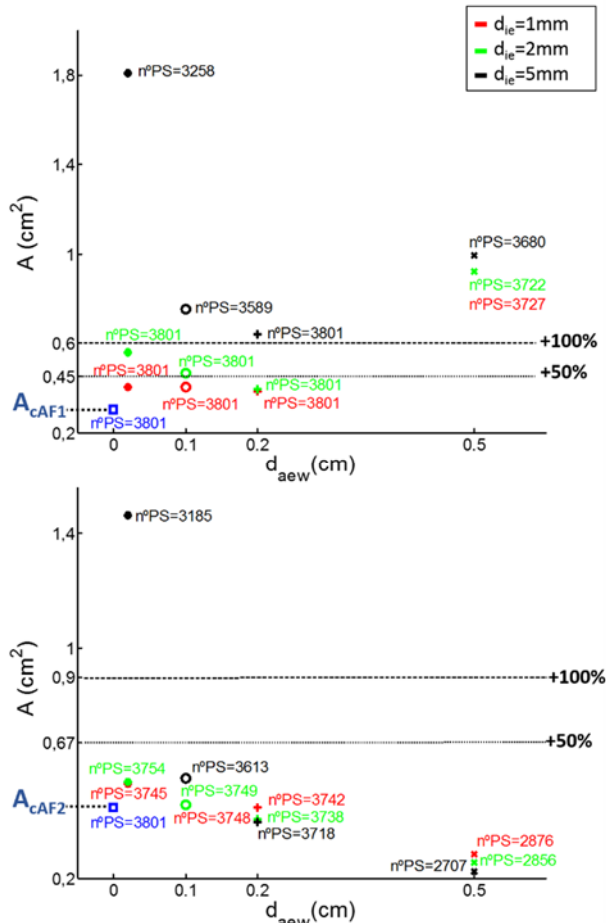

Figure 2. Meandering area (A) detected in the atria and the multi-electrode array for the cAF1 (top) and cAF2 (bottom) simulations. nºPS is the total number of PS detections.

At a spatial resolution of 2 mm, increasing the d_{aew} ($\leq$2 mm) decreased the detected meandering area at the array, but maintained it almost always equal or higher than in the atrium (A_{cAF1} was 0.56 for d_{ie}=1 mm, 0.47 cm^2 for d_{ie}=2 mm and 0.40 cm^2 for d_{ie}=5 mm. A_{cAF2} was 0.54 cm^2 for d_{ie}=1 mm, 0.45 cm^2 for d_{ie}=2 mm and 0.40 cm^2 for d_{ie}=5 mm). For d_{aew}>2mm, results are similar to those obtained for a spatial resolution of 1 mm.

Finally, at a spatial resolution of 5 mm, in case of the cAF1 simulation, the meandering area differed significantly from that in the atria, as well as the number of PS detections, regardless of the array-to-endocardial wall distance. Otherwise, in case of cAF2, the meandering area and number of PS detections was

significantly different for a d_{aew} of 0.2 and 5 mm, whereas they were similar for a d_{aew} of 1 and 2 mm. In fact, the array recognized the presence of the rotor as evidenced by a high number of PS detections (nºPS$\geq$2707), but it was not able to detect its trajectory accurately (see Figure 2 and Table 2).

Table 2. Shape of the meandering area detected in the atria and at the arrays for both simulations.

4.   Discussion

The results show that a stable rotor and its meandering trajectory can be detected accurately with a spatial resolution of $\leq$2 mm, as long as the array-to-endocardial wall distance is lower than 5 mm. For poorer spatial resolutions a stable rotor could be detected but its meandering trajectory would be untraceable. Our results agree with those of Rappel and Narayan [16], who maintain that a spatial resolution of up to 1 cm enables rotor localization. However, our data indicate that at such

a resolution the shape and size of the meandering area are unreliable. Nevertheless if a rotor is relatively stable and has a small meandering area (e.g., ~5-7 mm in diameter), better resolution might be of little clinical importance; i.e., as long as the center of rotation is detected the whole meandering area could be ablated since a single ablation lesion produces a crater of 5-7 mm in diameter [3].

It would be of interest to carry out further studies aimed at quantifying the required spatial resolution of the multi-electrode basket arrays to accurately track unstable rotors with large meandering areas. Such studies would provide rigorous evaluation of the clinical relevance, or lack thereof, when there is loss of information by using a spatial resolution of ≥5 mm, particularly when the ablation lesion fails to cover completely the rotor meandering region.

5. Conclusion

We conclude that the use of interpolated phase analysis of AF dynamics using multi-electrode arrays should consider that increasing the inter-electrode distance or the array-to-wall distance to ≤5 mm reduces precision in tracking a rotor trajectory, but does not preclude rotor identification.

Acknowledgements

References

[1] Montes-Santiago J, Rodil V, Formiga F, Cepeda JM, Urrutia A. Características y costes de los pacientes ingresados por arritmias cardiacas en España. Revista Clínica Española 2013;213:235-9.

[2] Fuster V, Rydén LE, Cannom DS, Crijns HJ, Curtis AB, Ellenbogen KA, et al. ACC/AHA/ESC 2006 guidelines for the management of patients with atrial fibrillation– executive summary: A report of the American College of Cardiology/American Heart Association Task Force on practice guidelines and the European Society of Cardiology Committee for Practice Guidelines (Writing Committee to Revise the 2001 Guidelines for the Management of Patients with Atrial Fibrillation) Developed in collaboration with the European Heart Rhythm Association and the Heart Rhythm Society. European heart journal. 2006; 27:1979-2030.

[3] Narayan SM, Krummen DE, Shivkumar K, Clopton P, Rappel WJ, Miller JM. Treatment of atrial fibrillation by the ablation of localized sources: CONFIRM (Conventional Ablation for Atrial Fibrillation With or Without Focal Impulse and Rotor Modulation) trial. J Am Coll Cardiol 2012;60:628-36.

[4] Umapathy K, Nair K, Masse S, Krishnan S, Rogers J, Nash MP, et al. Phase mapping of cardiac fibrillation. Circulation Arrhythmia and electrophysiology 2010;3:105-14.

[5] Tobón C, Ruiz-Villa C, Heidenreich E, Romero L, Hornero F, Saiz J. A three-dimensional human atrial model with fiber orientation. electrograms and arrhythmic activation patterns relationship. PLoS ONE 2013;8:e50883,1-13.

[6] Zipes DP, Jalife J. Cardiac electrophysiology: from cell to bedside (Sixth Edition). Philadelphia: Elsevier; 2014:351–9.

[7] Courtemanche M, Ramirez RJ, Nattel S. Ionic targets for drug therapy and atrial fibrillation-induced electrical remodeling: insights from a mathematical model. Cardiovascular Research 1999;42:477-89.

[8] Van Wagoner DR. Electrophysiological Remodeling in Human Atrial Fibrillation. Pacing and Clinical Electrophysiology. 2003;26:1572-5.

[9] Heidenreich EA, Ferrero JM, Doblare M, Rodriguez JF. Adaptive macro finite elements for the numerical solution of monodomain equations in cardiac electrophysiology. Annals of Biomedical Engineering 2010;38:2331-45.

[10] Ferrero Corral JM, Ferrero JM, Saiz J, Arnau A. Bioelectrónica: Señales bioeléctricas: SPUPV; 1994.

[11] Bray MA, Wikswo JP. Considerations in phase plane analysis for nonstationary reentrant cardiac behavior. Physical review E, Statistical, nonlinear, and soft matter physics 2002;65:051902.

[12] Gray RA, Pertsov AM, Jalife J. Spatial and temporal organization during cardiac fibrillation. Nature 1998;392(6671):75-8.

[13] Warren M, Berenfeld O, Guha P, et al. IK1 blockade reduces frequency, increases organization and terminates ventricular fibrillation in the guinea pig heart. PACE 2001;24:647.

[14] Bray MA, Lin SF, Aliev RR, Roth BJ, Wikswo JP, Jr. Experimental and theoretical analysis of phase singularity dynamics in cardiac tissue. Journal of Cardiovascular Electrophysiology 2001;12:716-22.

[15] Rogers JM. Combined phase singularity and wavefront analysis for optical maps of ventricular fibrillation. IEEE Transactions on Bio-Medical Engineering 2004;51:56-65.

[16] Rappel WJ, Narayan SM. Theoretical considerations for mapping activation in human cardiac fibrillation. Chaos 2013;23:023113.

Address for correspondence:

Laura Martínez Mateu
Instituto Interuniversitario de Investigación en Bioingeniería y Tecnología Orientada al Ser Humano (UPV). Ciudad Politécnica de la Innovación (Cubo Azul, Edif. 8B). Camino de Vera s/n, 46022 - Valencia (Spain).
laumarma@gbio.i3bh.es